POLISH MARITIME RESEARCH 4 (128) 2025 Vol. 32; pp. 4-19
10.2478/pomr-2025-0046

Investigation on the influence of inflow plane parameters on the prediction of full formed ship's self-propulsion performance

Feichi Gu[1), 2)]
Min Wang[1), 2)]
Long Zheng[1), 2)] *
Hao Wang [3)]
Shunhuai Chen[1), 2)]

[1)] School of Naval Architecture, Ocean and Energy Power Engineering, Wuhan University of Technology, China
[2)] Key Laboratory of High-Performance Ship Technology, Wuhan University of Technology, Wuhan, China
[3)] Hanjiang Nationnal Laboratory, China

* Corresponding author: *292171@whut.edu.cn (Long Zheng)*

ABSTRACT

The configuration of the inflow plane plays a critical role in self-propulsion simulations of ships using the body force method. In this study, we investigate the impact and applicability of different inflow plane settings on the self-propulsion simulation of a full-formed ship. A Reynolds-averaged Navier-Stokes (RANS) solver is used to simulate the self-propulsion of a full-formed ship model; by changing the inflow plane's parameters, simulation results under different conditions are obtained, and the influence of the inflow plane parameters on the self-propulsion simulation results is analysed. Based on the test results for the ship model, the optimal inflow plane parameters are identified using the TOPSIS method. Finally, the results are applied to the simulation of another full-formed ship. The calculated results obtained with the inflow plane parameter setting method proposed in this study are found to be more in line with the test results, and the calculation accuracy is better than with the conventional recommended parameter setting method. This study provides an effective suggestion for better use of the body force method to accurately predict the self-propulsion performance of a full formed ship.

Keywords: Body force; Self-propulsion; Inflow plane; Full-formed ship

INTRODUCTION

Following the trend towards the development of large-scale ships, full-formed ships with a block coefficient (C_b) larger than 0.85 have gradually come to predominate in terms of inland river ships. Compared to conventional ships with small C_b, prediction of the resistance performance of full formed ships is more susceptible to scale effects [1]. Due to the existence of separated flow in the flow field around the stern, numerical instability problems often arise in numerical calculations for full-formed ships such as commercial tankers and container ships [2]. This separated flow produces unsteady vortex structures (such as stern and bilge vortices), significantly increasing the nonlinear characteristics of the flow and resulting in the turbulence model. It is difficult to accurately capture the details of the separation zone. In order to improve the prediction accuracy of the resistance performance of full-formed ships, Peng et al. [3] proposed an improved Dawson method to improve the prediction of waveform and wave-making resistance of full-formed ships. Gong and Li [4] proposed a boundary element method based on Taylor expansion to predict the resistance and flow around a full-formed ship. However, compared with the ship's resistance, prediction of self-propulsion performance is more complicated, and at present, efficient and accurate prediction of the self-propulsion performance of full-formed ships is still a challenge.

Prediction of ship self-propulsion mainly relies on an analysis of the interaction between hull and propeller. Common methods currently in use include computational fluid dynamics (CFD) [5], hybrid models [6], model testing [7], and mechanical learning [8], among others. The use of a CFD method to predict ship self-propulsion can reduce the development cost and period for a new hull form; this is a mainstream approach, and many researchers have devised improvements to the CFD method, such as coupling with a Taylor expansion boundary element method (TEBEM) method [9]. In a CFD self-propulsion simulation, the calculations for the propeller are more complicated than for the hull resistance, and researchers generally use a discrete propeller method (DPM) [10] or body force method (BFM) [11] to simulate the propeller. Compared with BFM, DPM improves the calculation accuracy, but it also involves a higher mesh density and smaller time step, so the cost required for convergence is high [12]. BFM has a significant advantage in simulations of the flow conditions where there is no need for detailed flow conditions near the propeller; since it does not require specific meshing of the propeller, the total number of grid cells is greatly reduced, thereby reducing the time required to obtain the results.

BFM is widely applied in research involving ship self-propulsion simulations. Knight et al. [13] developed an unsteady body force propeller model using the BFM and a semi-empirical algorithm. Chuan et al. [14] used BFM to simulate the propeller behind the ship when exploring the influence of trim on ship performance. Zhang et al. [15] used BFM to study and analyse the interactions between the ship, propeller and rudder of a KRISO Container Ship (KCS) scalar model in still water. In addition, BFM can be used to predict the characteristic parameters of wave turning manoeuvring motion [16], and to study the influence of initial stability GM change on manoeuvring motion [17].

Compared with DPM, BFM reduces the computational cost, but its calculation accuracy is still deficient compared with DPM [10]. In order to improve the accuracy of the body force calculation, many researchers have proposed correction and optimisation methods for BFM. Guo et al. [18] proposed a new non-nested body force iteration method, which has excellent computational efficiency. Feng et al. [19] proposed a new physical model coupled with blade element momentum theory, and used this model to simulate KCS self-propulsion. Their simulation results were very close to both experimental and DPM simulation results. Cai et al. [20] proposed a ducted virtual disc method for the ducted propellers of trawlers, in which the traditional BFM was modified, and found that this improved the accuracy of the ducted propeller calculation. Yu et al. [21] proposed an improved BFM called OUM to accurately predict full-scale KCS self-propulsion.

The most commonly used body force optimisation methods generally involve modifying the function used or changing the distribution method for the force and moment. The purpose of both approaches is to bring the calculation results closer to those obtained from DPM or test results, but this invariably requires a significant time cost, and some corrections are not applicable to ordinary types of propellers. In engineering projects that involve numerous calculations, both DPM and the modification methods described above are unrealistic; some researchers have therefore considered the influence of the inflow plane on the research results when using BFM. Aram and Mucha [22] selected a value for the inflow plane offset of 0.16–0.2 times the radius of the propeller when studying the self-propulsion of the ship ONRTH5613. Xie et al. [23] analysed the influence of the inflow plane offset on the self-propulsion of a Panamanian bulk carrier model in an area of ice. The study showed that when the inflow plane offset is 0.04–0.2 times the radius of the propeller, it has little effect on the open water results of the propeller. It is therefore recommended that the inflow plane offset be less than 0.2 times the radius of the propeller. Cai et al. [24] chose an inflow plane radius of 1.1 times the propeller radius when studying the self-propulsion of KVLCC.

In the research work described above, the setting of the inflow plane has been considered but the impact on the self-propulsion simulation has not been explored in detail, and researchers have typically referred to recommended values obtained from guidelines in commercial software [25] for the setting of parameters. However, when BFM is used for simulation calculations of full-formed ships, there is no quantitative analysis that indicates whether such inflow plane parameter settings are applicable.

In summary, the BFM is used in this study to predict the self-propulsion of a full-formed ship, and the influence of the inflow plane parameters is explored. A self-propulsion simulation is carried out under different inflow plane parameter settings, and the results are compared with those from model tests. The optimal inflow plane parameter setting is obtained, and the influence of the parameters is analysed. The findings from this research are applied to the simulation of another full-formed ship to verify their applicability. This study provides a theoretical basis for the better use of BFM to accurately predict the self-propulsion performance of a full-formed ship.

The remainder of the paper is organised as follows. Section 2 describes the research object considered in this study, the numerical method used, and the settings for the solver. Section 3 presents an assessment of the reliability of the simulation results based on the independence of the solver and the accuracy of the results. In Section 4, we explore the influence of changes to the inflow plane parameters on the simulation and the selection of optimal inflow plane parameters. Section 5 verifies the universality of the optimal parameters on the hull form.

MATERIALS AND METHODS

RESEARCH OBJECT

The research object is a 5000-ton inland twin-propeller ship with a length-to-width ratio of 5.65, a width-to-draft ratio of 2.81, and a block coefficient of 0.9, representing a full-formed ship. The ship's propeller is a Wageningen B series. The main parameters of the ship model and propeller are shown in Table 1. Conversion of the Reynolds number between the full-scale ship and the model is done at the operating speed. The test model and the three-dimensional modelling scheme are shown in Fig. 1, and the results of open water tests of the propeller are shown in Fig. 2, where the propeller advance coefficient J and thrust coefficient K_T, torque coefficient K_Q are the dimensionless parameters of the propeller performance. The expressions for the Reynolds number and propeller parameters are given in Eqs. (1) to (4):

$$Re = \frac{V \cdot C}{\boldsymbol{\nu}} \tag{1}$$

$$J = \frac{V_A}{nD} \tag{2}$$

$$K_T = \frac{T}{\rho n^2 D^4} \tag{3}$$

$$K_Q = \frac{Q}{\rho n^2 D^5} \tag{4}$$

where v is the fluid velocity, C is the characteristic length, and $\boldsymbol{\nu}$ is the kinematic viscosity of the fluid. V_A is the advance speed (that is, the speed of the propeller along the axis direction), n is the propeller speed, D is the propeller diameter, T and Q are the thrust and torque of the propeller respectively,ρ is the density, and η_{0m} is the propeller efficiency.

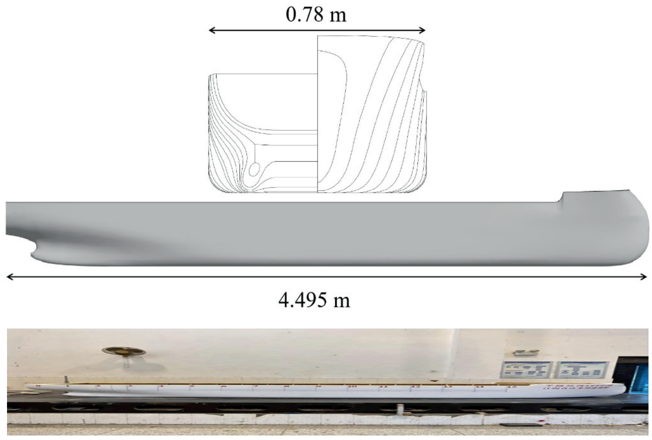

Fig. 1. Three-dimensional simulation model and model used for tests

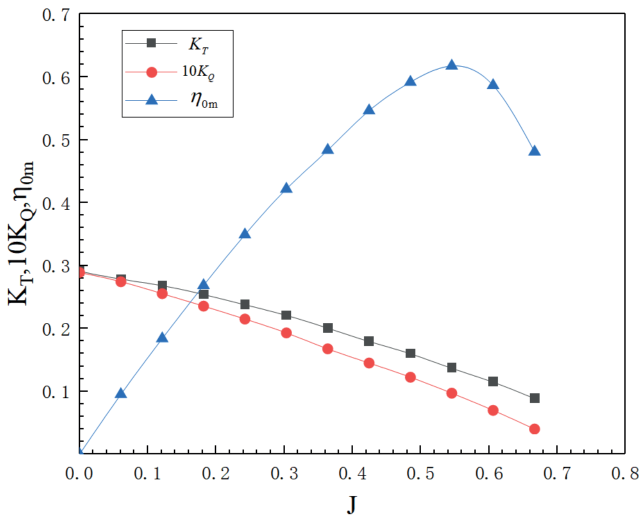

Fig. 2. Results of open water tests of the propeller

Tab. 1. Main parameters of the ship model and propeller

Hull				
Parameter	**Symbols**	**Units**	**Full-scale**	**Model**
Waterline length	L_{wl}	m	89.90	4.495
Length between Perpendiculars	L_{pp}	m	89.90	4.495
Beam	B	m	15.6	0.78
Draft	T	m	5.55	0.2775
Displacement	Δ	t	6152.8	0.7691
Reynolds number	R_e		4.42×10^8	4.94×10^6
Block coefficient	C_b		0.9	
Propeller				
Propeller type	B			
Propeller diameter	D	m	3.20	0.160
Blade area ratio	A_E/A_0		0.55	
Pitch ratio	$P_{0.7}/D$		0.68	
Number of blades	Z		4	
Skew angle	θ	deg	16	
Rake angle	ε	deg	15	
Hub diameter ratio	0.18			
Scale ratio	λ		20	

CONTROL EQUATIONS AND TURBULENCE MODELS

In an incompressible flow field, the control equations for the fluid are the continuity equation and the momentum equation. The most commonly used RANS method is based on the Boussinesq assumption, and is a time homogenisation treatment of the Navier–Stokes (N-S) equation (momentum equation). As long as the Reynolds stress phase is solved in the treated equation, the N-S equation can be closed.

The continuity and momentum equations are given in Eqs. (5) and (6):

$$\frac{\partial u_i}{\partial x_i} = 0 \tag{5}$$

$$\rho\left(\frac{\partial u_i}{\partial t} + u_j\frac{\partial u_i}{\partial x_j}\right) = -\frac{\partial \bar{p}}{\partial x_i} + \frac{\partial}{\partial x_j}\left(\mu\frac{\partial u_i}{\partial x_j} - \rho\overline{u_i'u_j'}\right) + \rho\overline{f_i} \tag{6}$$

where $u_i (i = 1,2,3)$ are the components of the Reynolds time-averaged velocity vector, ρ is the density, $\bar{p}$ is the average pressure, μ is the dynamic viscosity, $\overline{u_i'u_j'}$ is Reynolds stress, and $\overline{f_i}$ is the body force.

In order to solve for the Reynolds stress term, the most frequently used method in engineering is to use the k-ε two-equation model. By solving for the turbulent kinetic energy k and the turbulent dissipation ε, the Reynolds stress term is indirectly solved to close the momentum equation, and the k-ε model can be realised. The modified transport equation for the dissipation rate ε is derived from the exact equation for the mean square vorticity fluctuation. The normal stress is mathematically constrained to ensure that the flow conforms to the physical rule of turbulence. The equations are given in Eqs. (7) to (13):

$$\frac{\partial(\rho k)}{\partial t} + \frac{\partial(\rho k u_i)}{\partial x_i} = \frac{\partial}{\partial xj}\left[\left(\mu + \frac{\mu_t}{\sigma_k}\right)\frac{\partial k}{\partial x_j}\right] + G_k - \rho\varepsilon + S_k \tag{7}$$

$$\frac{\partial(\rho\varepsilon)}{\partial t} + \frac{\partial(\rho\varepsilon u_i)}{\partial x_i} = \frac{\partial}{\partial xj}\left[\left(\mu + \frac{\mu_t}{\sigma_\varepsilon}\right)\frac{\partial \varepsilon}{\partial x_j}\right] + \rho C_1 S\varepsilon - \rho C_2\frac{\varepsilon^2}{k+\sqrt{v\varepsilon}} + S_\varepsilon \tag{8}$$

$$\mu_t = C_\mu \rho\frac{k^2}{\varepsilon} \tag{9}$$

$$G_k = \tau_{ij}\frac{\partial u_i}{\partial x_j} \tag{10}$$

$$S = \sqrt{2s_{ij}s_{ij}} \tag{11}$$

$$C_1 = \max\left[0.43, \frac{\eta}{\eta+5}\right] \tag{12}$$

$$\eta = S\frac{k}{\varepsilon} \tag{13}$$

where μ_t is the turbulent viscosity, G_k is the kinetic energy generated by the mean velocity gradient, τ_{ij} is the Reynolds stress tensor, σ_k and σ_ε are constants, C_μ , $C_{1\varepsilon}$ and $C_{2\varepsilon}$ are coefficients determined from experiments on basic turbulence, S is a scalar measure of the strain rate tensor, v is the kinematic viscosity, C_1 and C_2 are the model constants: $C_2 = 1.9$, $\sigma_k = 1.0$, $\sigma_\varepsilon = 1.2$.

BODY FORCE METHOD

In BFM, the thrust is distributed in a cylindrical area defined by the diameter of the propeller disc and the longitudinal thickness of the propeller according to the change in radius, to establish a virtual propeller. A schematic diagram of the virtual propeller at the stern is shown in Fig. 3, where its spatial position is exactly the same as in the actual propeller arrangement.

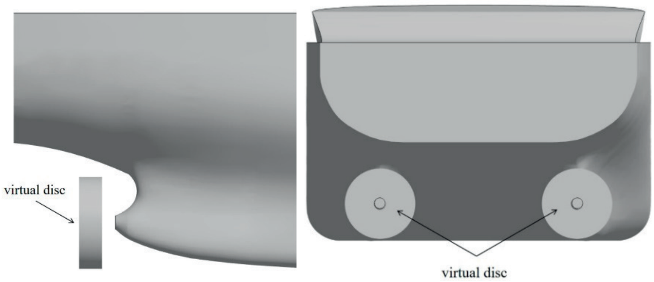

Fig. 3. Schematic diagram of the virtual disc

The thrust and torque of the virtual propeller are interpolated on the open water performance curve according to the average speed of the inflow plane in front of the propeller. The axial force and tangential force distribution on the virtual propeller are optimised using the Goldstein method [26] proposed by Hough and Ordway [27]. Eqs. (14) to (20) give the mathematical expressions used here.

$$f_{bx} = A_x r^*\sqrt{1-r^*} \tag{14}$$

$$f_{b\theta} = A_\theta\frac{r^*\sqrt{1-r^*}}{r^*(1-r_h{}')+r_h{}'} \tag{15}$$

$$r^* = \frac{r'-r_h{}'}{1-r_h{}'} \tag{16}$$

$$r_h{}' = \frac{R_H}{R_P} \tag{17}$$

$$r' = \frac{r}{R_P} \tag{18}$$

$$A_x = \frac{105}{8}\cdot\frac{T}{\pi\Delta(3R_H+4R_P)(R_P-R_H)} \tag{19}$$

$$A_\theta = \frac{105}{8}\cdot\frac{Q}{\pi\Delta R_P(3R_H+4R_P)(R_P-R_H)} \tag{20}$$

where f_{bx} is the axial force; $f_{b\theta}$ is the tangential force; R_P is the radius of the propeller; R_H is the radius of the hub; r is the radius of radiation; and T, Q are the thrust and torque of the open water propeller, respectively.

The shape of the virtual disc is similar to a hollow cylinder. The radius of the outer cylinder (i.e. the outer radius of the virtual disc) is the same as the radius of the propeller R_p, and the inner radius is the same as the radius of the propeller hub R_H. The thickness is usually set to that of the propeller, and all of the geometric parameters should correspond to those of the propeller. The positional relationship between the inflow plane and the virtual disc is shown in Fig. 4. The inflow plane can be understood as a circular inflow surface in front of the virtual propeller (shown as a blue line in Fig. 4). The centre of the circle is located at the centre of the propeller shaft. The geometric radius of the circular surface is defined as the radius r' of the inflow plane [25], and the value is usually a percentage of the propeller radius R_p (90% R_p in Fig. 4). The distance from the circular surface to the body force cylinder is defined as the offset ΔL of the inflow plane [25], and the value is also a percentage of the propeller radius R_p (15% R_p in Fig. 4).'

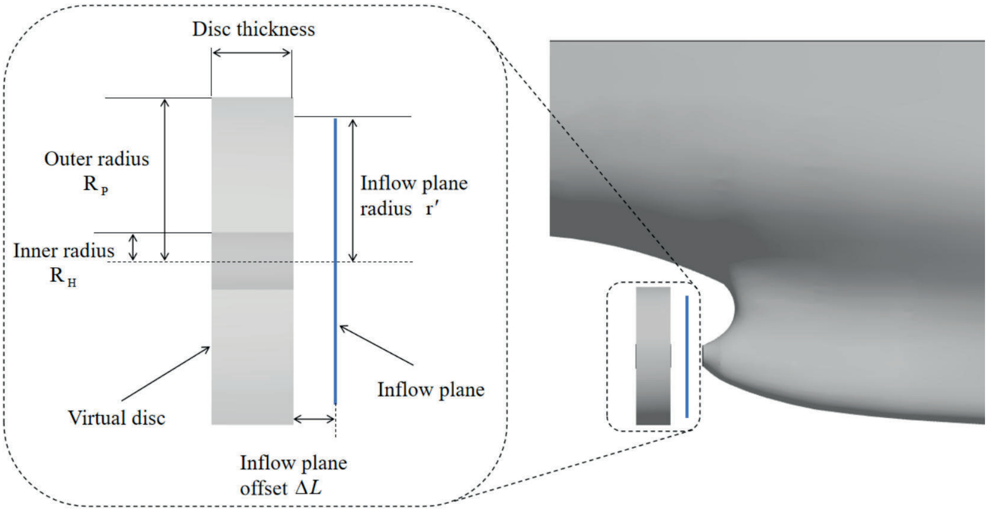

Fig. 4. Parameters of the virtual disc and inflow plane

SELF-PROPULSION CALCULATION

In this study, the self-propulsion simulation is carried out with BFM. The specific process used for the self-propulsion calculation is illustrated in Fig. 5. The open water results are added to the virtual propeller, and the inflow plane radius and inflow plane offset are set as the input values. Under a certain speed V_A, the thrust T, torque Q and resistance R of the ship model can be calculated by changing the propeller speed n.

Based on the principle of equal thrust, the equilibrium point thrust and virtual propeller rps (revolutions per second) are obtained. The equilibrium equation is shown in Eq. (21). When the net force $T_e = 0$, this is the self-propulsion point for the ship model:

$$T_e = \mathrm{T} - \mathrm{R} - t \cdot T + \mathrm{F}_D \tag{21}$$

where t is the thrust reduction coefficient, $t \cdot \mathrm{T}$ is the thrust deduction resistance, and F_D is the correction value of frictional resistance between the real ship and the ship model, which is obtained by combining the resistance simulation results with those of the two-dimensional method. The simulation results at different speeds can be plotted to obtain curves for R and T. The intersection of the model ship's resistance ($\mathrm{R}-\mathrm{F}_D$) curve and the T curve after deducting the correction value for the frictional resistance gives the self-propulsion point of the sample point, from which the self-propulsion point thrust and speed can be calculated.

The aim of this self-propulsion simulation was to comprehensively analyse the propulsion efficiency components (shown in green in Fig. 5). The influence of the propeller on the ship is shown as the thrust reduction t in Eq. (22), where R_m is the resistance value of the ship model obtained from a resistance simulation at the corresponding speed for the ship model. The wake fraction ω represents the influence of the ship on the propeller. The expression for ω is shown in Eq. (23), where V is the speed of the ship model, and the propeller efficiency η_{0m} of the self-propulsion point is obtained from the open water curve based on the thrust coefficient K_T of the self-propulsion point. The hull efficiency η_{Hm} is the efficiency to measure the influence of the hull in the working environment of the propeller. The expression for η_{Hm} is shown in Eq. (24). The relative rotation efficiency η_{Rm} is the ratio of the propeller's after-ship efficiency to its open water efficiency, as shown in Eq. (25), where η_{Bm} is the propeller's after-ship efficiency. The BFM does not directly simulate the rotating flow field of the propeller, and cannot capture the energy loss of a real propeller in the non-uniform flow field of the stern ($\eta_{Bm} = \eta_{0m}$), which is equivalent to the default flow field. The model is ideal, so the relative rotation efficiency η_{Rm} has a value of one. The propulsion efficiency η_D represents how much of the power the propeller receives is actually used to push the hull forward; the expression for η_D is shown in Eq. (26).

$$t = \frac{T - R_m}{T} \tag{22}$$

$$\omega = 1 - \frac{JnD}{V} \tag{23}$$

$$\eta_{Hm} = (1 - t)/(1 - \omega) \tag{24}$$

$$\eta_{Rm} = \frac{\eta_{Bm}}{\eta_{0m}} \tag{25}$$

$$\eta_D = \eta_{0m} \cdot \eta_{Hm} \cdot \eta_{Rm} \tag{26}$$

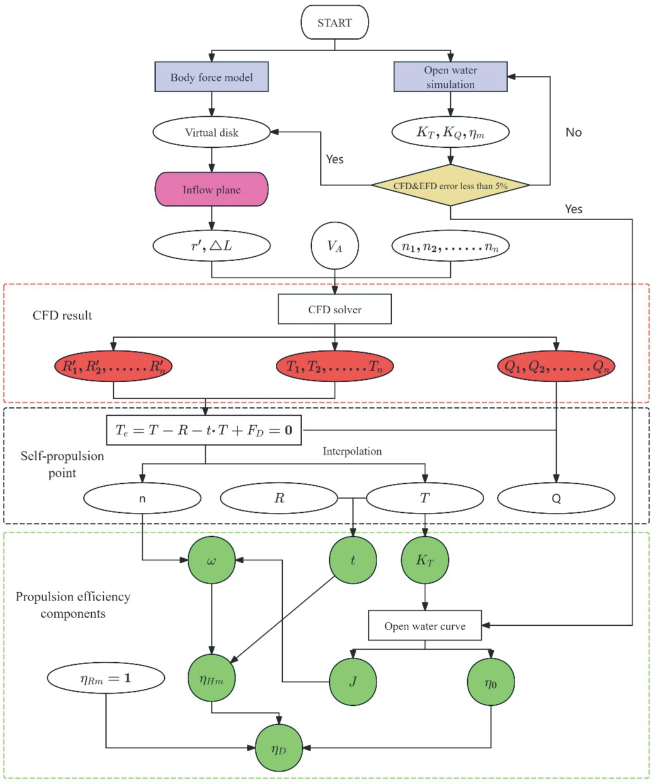

Fig. 5. Flowchart for the self-propulsion computation

CFD SOLVER SETTINGS

The simulation was carried out using the commercial software STAR-CCM+, and the calculation domain is shown in Fig. 6. Since a twin-propeller ship is considered here, the calculation domain was selected as a half-ship in order to reduce the calculation cost. The inlet, side wall, top and bottom of the calculation domain were defined as the velocity inlet, the outlet was defined as the pressure outlet, and the centre plane was set as a symmetrical plane. Two-phase flow theory was used to set the boundary conditions. The velocity inlet should be 1.0 L_{PP} away from the hull, and the pressure outlet should be 3.0 L_{PP} away from the hull. Wave attenuation was set at the entrance, exit and side wall, with a wave attenuation wavelength of 1.0 L_{pp}. In the physical model setting, the value of the incoming flow velocity was set to the plate VOF wave velocity, and the value of the ambient pressure was set to the hydrostatic pressure of the plane VOF wave.

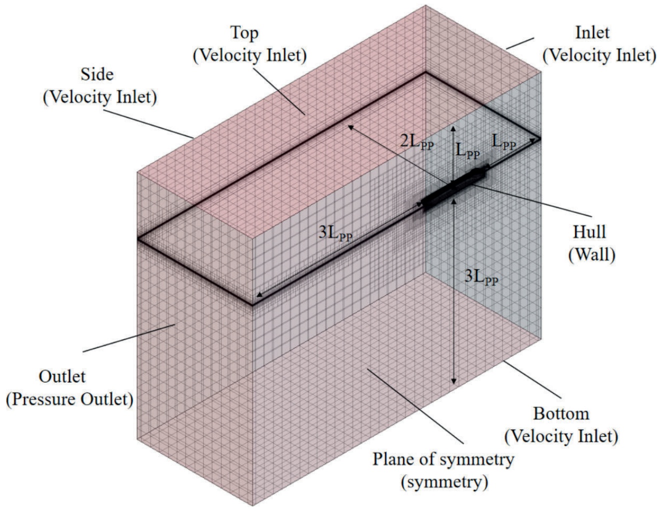

Fig. 6. Computational domain and boundary conditions

Since it is not necessary to create a grid for the propeller, the difference between the grid and the conventional resistance is only the refinement at the virtual disc. Hence, taking the grid for the resistance simulation as an example, the calculation area was discretised by the finite body method, and the grid was generated based on STAR-CCM+. Following the requirements of ITTC, the free surface area and the Kelvin wave area were refined in three layers, and the grid of the hull surface and the bow and stern were refined. The grid size was based on the $L_{PP}/50$ value, and the boundary layer thickness was calculated according to the specific selected ship conditions and turbulence model. The total number of grid cells was 2.9 million. The mesh grid is shown in Fig. 7.

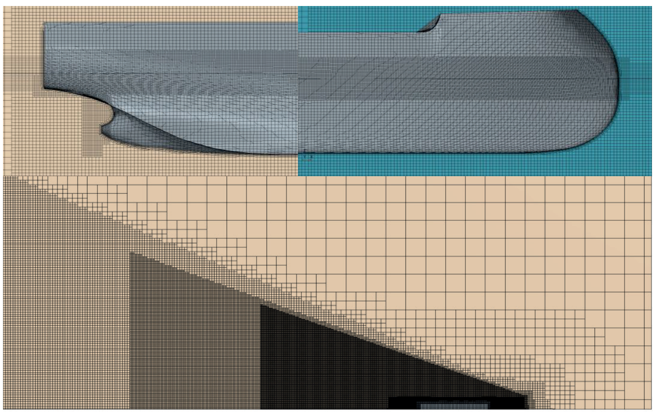

Fig. 7. Grid configuration

SOLVER VERIFICATION

IRRELEVANT VERIFICATION

The verification method proposed by Stern [28] was used to verify the independence of the grid used in the calculation.

With a time step of 0.02 s, according to the ratio of $\sqrt{2}$, the two sets of grids were divided into three groups representing fine, medium and coarse meshes. Table 2 shows the number of grid corresponding to the three sets of grids. The independence of time step size was verified at the grid size of the medium mesh. Time steps were similarly divided into three sizes at a ratio of $\sqrt{2}$, with $t_1 = 0.014\ s$, $t_2 = 0.020\ s$, and $t_3 = 0.028\ s$.

Tab. 2. Grid size and total number of grid cells

Grid configuration	Base size (mm)	Number of cells (million)
Fine	56	6.43
Medium	80	3.19
Coarse	113	1.26

The convergence results for the grid and time step are shown in Tables 3 and 4 according to Richardson's extrapolation method, where S_i (i=1, 2, 3) is the calculation result for the ship model's resistance R under the corresponding grid, which is the grid magnification and the convergence factor mentioned in Stern's literature. S_C represents the corrected simulation results. U_C is the corrected uncertainty, and δ^* is the corrected value. It can be seen from Tables 3 and 4 that the calculation results for R are sensitive to the grid size, and it can be considered that the grid size and the selected time step are reliable.

Tab. 3. Results of grid independence verification

r_G	$Fine(S_1)$	$Medium(S_2)$	$Coarse(S_3)$	R_G	$\%\delta_G{}^*$	$\%U_G{}^*$	$\%\delta_{CG}{}^*$
$\sqrt{2}$	7.368	7.369	7.410	0.025	10.692	0.003	0.003

Tab. 4. Results of time step independence verification

r_G	$Fine(t_1)$	$Medium(t_2)$	$Coarse(t_3)$	R_T	$\%\delta_T{}^*$	$\%U_T{}^*$	$\%\delta_{CT}{}^*$
$\sqrt{2}$	7.369	7.369	7.370	0.111	6.340	0.001	0.002

ACCURACY VERIFICATION

In order to verify the accuracy of the grid, corresponding model tests were also carried out in the towing tank of Wuhan University of Technology (Fig. 8). The total length of the tank was 132 m, the width was 10.8 m, and the depth was 2 m. The maximum speed of the trailer was 7.2 m/s, where the adjustable trailer speed was automatically controlled by a computer closed-loop, and the speed stabilisation accuracy was 1%. The main measuring instruments were as follows: Cussons R63 drag meter, Cussons R135, R136 propeller power meter, variable-frequency speed regulation controller, and HBM signal amplifier MP55. At a 95% confidence level (k = 2), the total resistance of each speed and the expanded uncertainty of its main hydrodynamic coefficients were all less than 1.1%.

We carried out a resistance test of the ship model under design draft, an open water test of the propeller, and a self-propulsion test of the ship model under design draft. In both the resistance test and the self-propulsion test, an operating speed of V = 1.035 m/s was selected (ship model speed), and the water temperature was 21.6°C. The results for the CFD simulation and the experimental fluid dynamics (EFD) tests were compared and analysed. A comparison of the resistance simulation results is shown in Fig. 9, and it can be seen that the simulation results are close to those of the experiments; the maximum error in the resistance is less than 5%, a finding that verifies the accuracy of the grid used in this study.

Fig. 8. Photograph of the towing tank

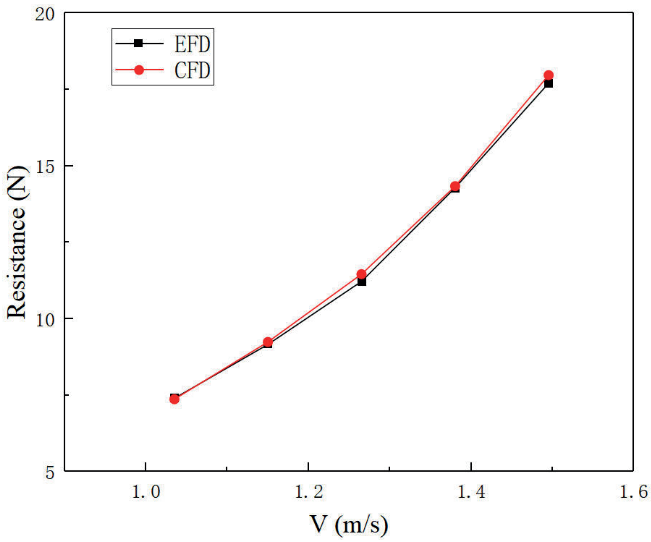

Fig. 9. Results of resistance simulations

RESULT AND DISCUSSION

SAMPLE POINT PARAMETER SETTING METHOD

In the STAR-CCM+ *Instructions for User* file [25], it is recommended that the inflow plane radius r' should be set to greater than 10% of the virtual propeller radius R_P, and the inflow plane offset ΔL should be 20% of the virtual propeller radius R_P, i.e. the values should be greater than 1.1 R_P and

0.2 R_p, respectively. Since the simulation object corresponding to the parameters of the flow plane recommended in these instructions is a narrow and thin ship, the recommended values are not applicable to a full-formed ship with C_b greater than 0.85. In order to improve the simulation calculation accuracy of self-propulsion performance prediction, it is therefore necessary to analyse settings for the inflow surface parameters that are suitable for full-formed ships.

In order to explore the influence of the inflow plane parameters, the value of the inflow plane radius r' is selected as 0.8–1.2 times the radius of the virtual propeller, and the value of the inflow plane offset ΔL is selected as 0.05–0.2 times the radius of the virtual propeller. According to the principle of mean distribution, Table 5 shows the values of the inflow plane parameters for each sample point, where R_p is the radius of the propeller.

In this work, we consider three propeller speeds of 8, 10, and 12 rps for the calculation of the self-propulsion point and the subsequent propulsion efficiency, as shown in Fig. 5. We first analysed the influence of the inflow plane, and then determined the best inflow plane parameter settings based on the self-propulsion factor obtained by conversion. This is described further in the following sections.

Tab. 5. Values of the inflow plane parameters for each sample point

Parameter	r'/R_p	$\Delta L/R_p$
Sample 1	0.8	0.05
Sample 2	0.8	0.125
Sample 3	0.8	0.20
Sample 4	0.9	0.05
Sample 5	0.9	0.125
Sample 6	0.9	0.20
Sample 7	1.0	0.05
Sample 8	1.0	0.125
Sample 9	1.0	0.20
Sample 10	1.1	0.05
Sample 11	1.1	0.125
Sample 12	1.1	0.20
Sample 13	1.2	0.05
Sample 14	1.2	0.125
Sample 15 (recommended)	1.2	0.20

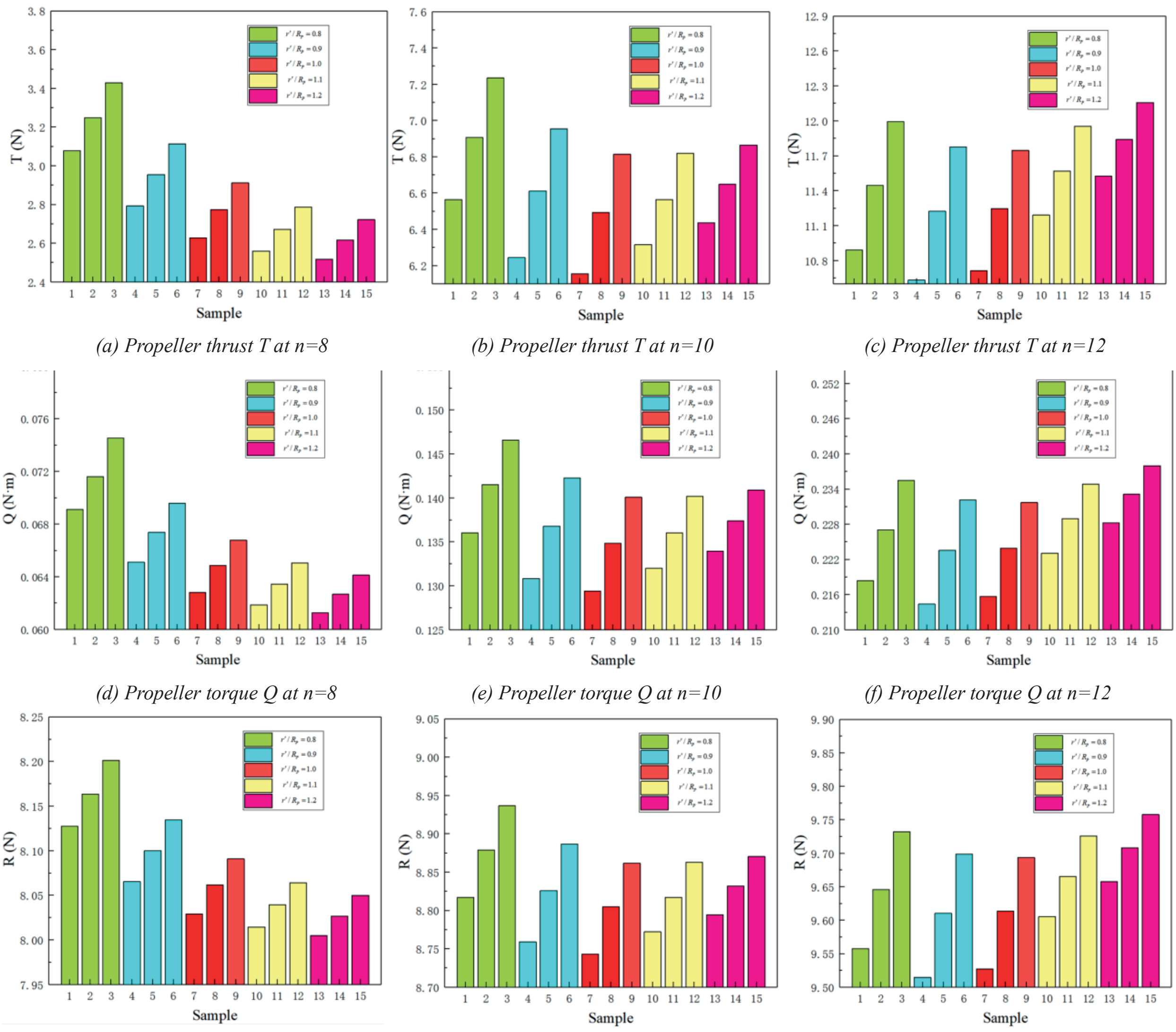

(a) Propeller thrust T at n=8 *(b) Propeller thrust T at n=10* *(c) Propeller thrust T at n=12*

(d) Propeller torque Q at n=8 *(e) Propeller torque Q at n=10* *(f) Propeller torque Q at n=12*

(g) Hull resistance R at n=8 *(h) Hull resistance R at n=10* *(i) Hull resistance R at n=12*

Fig. 10. Summary of self-propulsion results at different speeds for each sample point

INFLUENCE OF THE INFLOW PLANE

We explored the influence of the incoming flow plane on the self-propulsion results. Fig. 10 shows the values of the propeller thrust T, torque Q and hull resistance R monitored at all sample points at different propeller speeds in the simulations.

From the results in Fig. 10, we can obtain the following findings: (i) a change in the inflow plane parameters will affect the self-propulsion results, with a maximum difference reaching 36.25% (propeller thrust T, n=8, Samples 3 and 13); (ii) the influence of the inflow plane parameters on the propeller thrust T, torque Q and hull resistance R at the same propeller speed is equivalent, and the variation in these three monitoring values is consistent; (iii) for the same inflow plane radius, the self-propulsion simulation value (R, T, Q) generally shows an increasing trend with an increase in the inflow plane offset.

In order to evaluate the influence of a change in the inflow plane parameters on the wake field of the virtual propeller, we analysed the velocity field u/v at $0.1R_p$ behind the propeller, where u is the water velocity and v is the ship's velocity. Fig. 11 shows the effective wake diagram when the propeller speed n=10, and it can be seen that a change in the offset of the inflow plane has little effect on the axial velocity distribution, although it does have an effect on the peak velocity of the wake. With an increase in the inflow plane offset, the peak velocity increases. The peak value of the wake velocity for Sample 3 is the maximum for all samples.

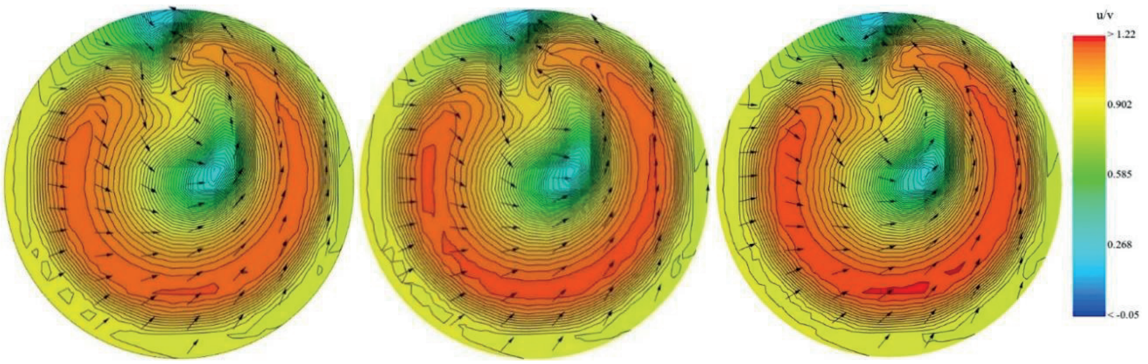

(a) Sample 1 *(b) Sample 2* *(c) Sample 3*

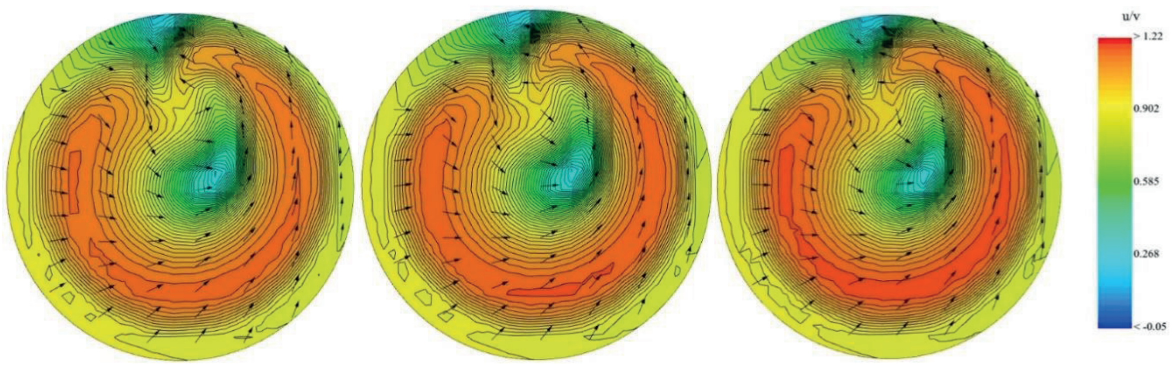

(d) Sample 4 *(e) Sample 5* *(f) Sample 6*

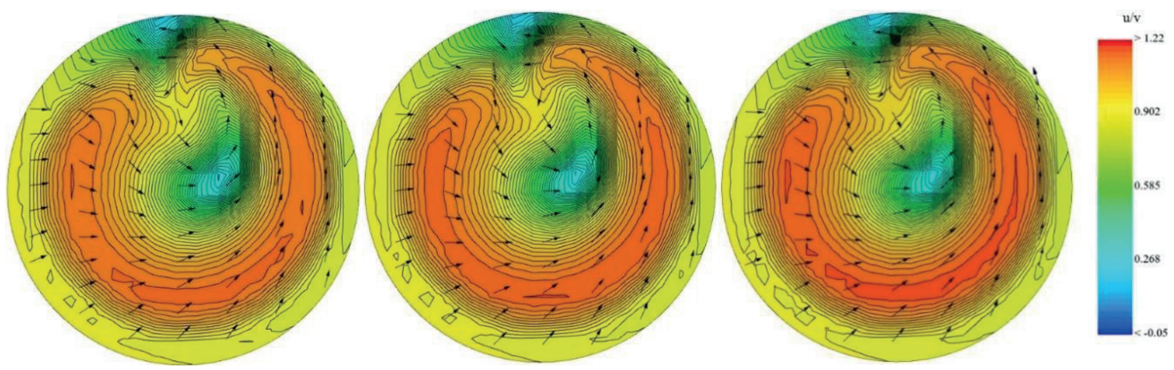

(g) Sample 7 *(h) Sample 8* *(i) Sample 9*

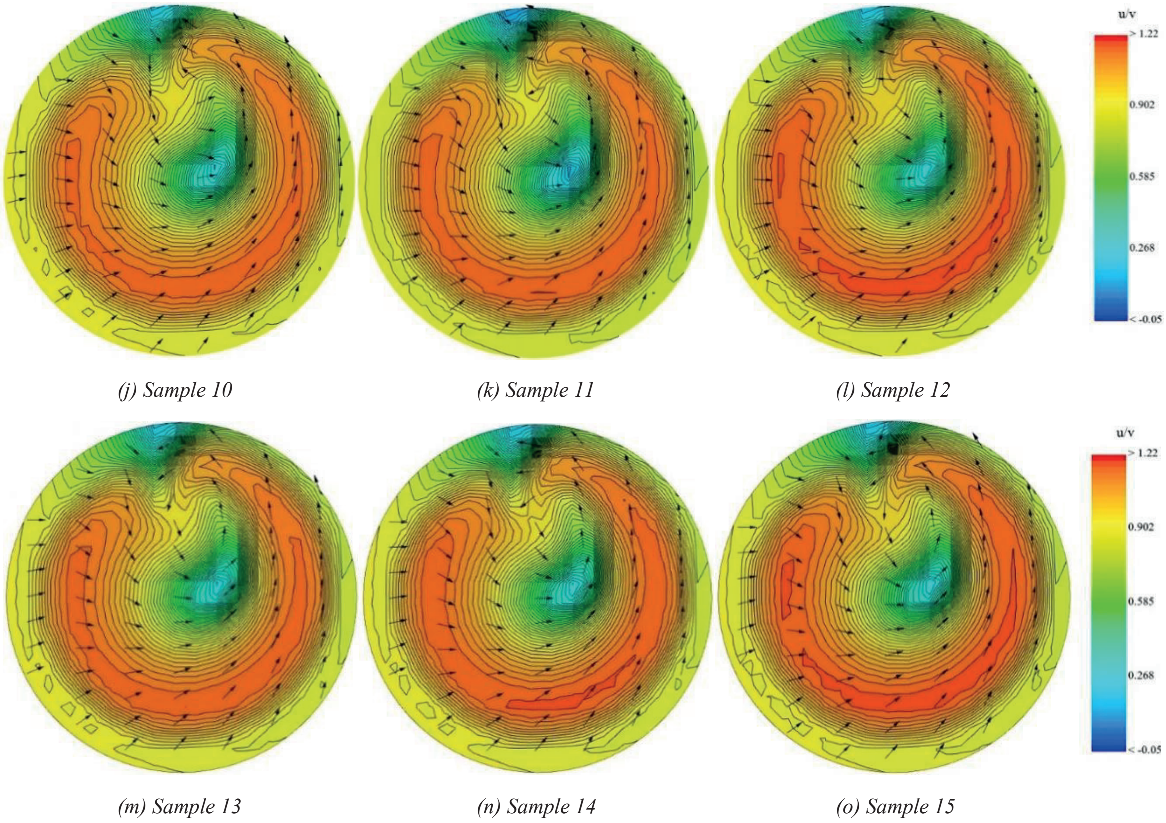

(j) Sample 10 *(k) Sample 11* *(l) Sample 12*

(m) Sample 13 *(n) Sample 14* *(o) Sample 15*

Fig. 11. Velocity fields u/v at 0.1RP behind the propeller n=10 rps, for all samples

OPTIMAL VALUES FOR THE RADIUS AND THE OFFSET OF THE INFLOW PLANE

In order to determine the optimal inflow plane parameters, we consider the CFD calculation results and EFD test results under different inflow plane parameters. Based on the conversion process shown in Fig. 5, the results for the self-propulsion factor (t, ω, η_{0m}, etc.) are obtained. The error in each CFD and EFD result is calculated using Eq. (27), and the error results are visualised in Fig. 12.

$$Error = \frac{|S_{CFD} - S_{EFD}|}{S_{EFD}} \tag{27}$$

It can be seen from Fig. 12 that when the radius of the inflow plane is greater than 1.1 times the radius of the virtual propeller (Samples 10 to 15), the error in each parameter is large. Sample 3 in Fig. 12(a) has the smallest proportion of area in the error diagram, but the optimal inflow plane parameters cannot be judged based on a single area proportion: for example, the errors in the thrust coefficient and propulsion efficiency for Sample 3 in Fig. 12(a) are greater than for Sample 2.

This means that the optimal inflow plane parameters cannot be judged based on the minimum error of a single index, and a comprehensive analysis method that takes into consideration multiple indices is needed. In this study, Technique for Order Preference by Similarity to Ideal Solution (TOPSIS) method was chosen to find the best parameters, as this is a classical multi-criteria decision analysis method.

The main factors affecting the propulsion efficiency in the self-propulsion calculation are the thrust reduction coefficient t, wake fraction ω and propeller efficiency η_{0m}. Based on these three indices, the interaction between the ship and the propeller can be analysed and the remaining factors affecting the propulsion efficiency can be obtained. We therefore used the TOPSIS method to analyse the error results for 15 sets of sample points for these three values. The results are shown in Table 6, where the closeness represents the error closeness: the smaller the value, the closer the sample to the positive ideal solution. The quantities t_{error}, ω_{error} and $\eta_{0merror}$ represent the errors between the simulation results and the experimental results for the three factors affecting the propulsion efficiency, which are given the same weight (1/3) in the TOPSIS method. Fig. 13 shows a distribution diagram of the closeness degree of the sample. It can be seen that Sample 3 is the best sample point; in other words, when the inflow plane parameter is set to $r' = 0.8R_p$ and $\Delta L = 0.2R_p$, this is the best parameter setting for the inflow plane under the comprehensive index. This parameter setting is superior to those given in the STAR-CCM+ *Instructions for User* file (Sample 15). Through the research work described above, we determined the inflow plane parameter setting suitable for our research ship type, i.e. the parameters of Sample 3, with an inflow plane radius $r' = 0.8R_p$ and offset $\Delta L = 0.2R_p$.

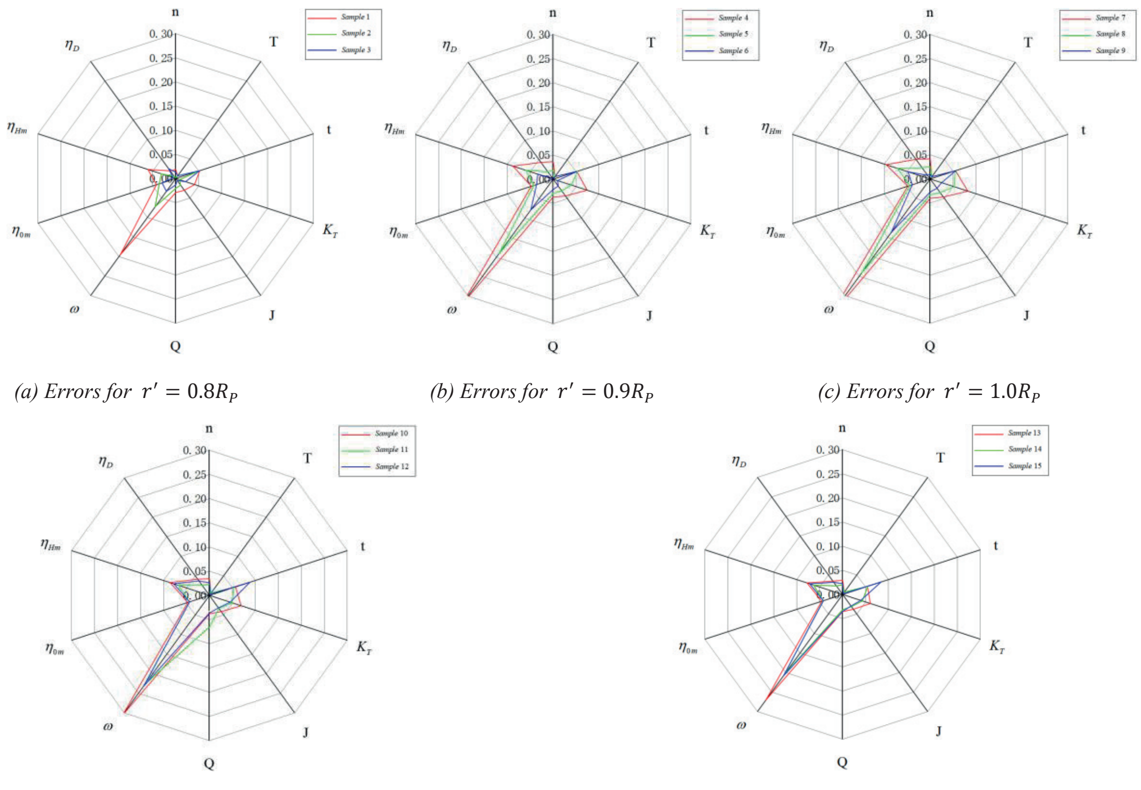

(a) Errors for $r' = 0.8R_P$ *(b) Errors for* $r' = 0.9R_P$ *(c) Errors for* $r' = 1.0R_P$

(d) Errors for $r' = 1.1R_P$ *(e) Errors for* $r' = 1.2R_P$

Fig. 12. Error analysis for each sample point

Table 6. Results of TOPSIS test

Parameter	t_{error}	ω_{error}	$\eta_{0merror}$	Closeness
Units	/	/	/	/
Sample 1	0.052	0.196	0.042	0.450
Sample 2	0.050	0.073	0.036	0.135
Sample 3	**0.052**	**0.033**	**0.030**	**0.020**
Sample 4	0.052	0.322	0.047	0.682
Sample 5	0.053	0.191	0.042	0.442
Sample 6	0.052	0.079	0.036	0.151
Sample 7	0.055	0.356	0.049	0.731
Sample 8	0.055	0.242	0.044	0.565
Sample 9	0.056	0.137	0.039	0.313
Sample 10	0.057	0.306	0.047	0.693
Sample 11	0.053	0.227	0.044	0.526
Sample 12	0.088	0.232	0.043	0.666
Sample 13	0.054	0.271	0.045	0.617
Sample 14	0.055	0.205	0.042	0.480
Sample 15 (recommended)	0.084	0.208	0.042	0.596

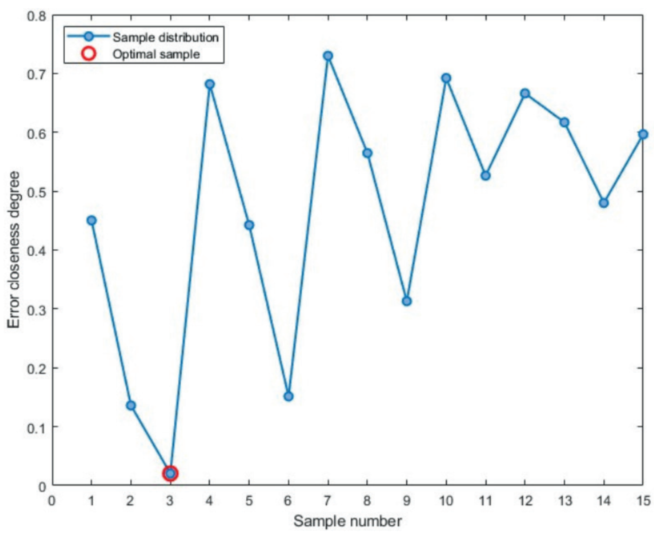

Fig. 13. The sample sorting result based on TOPSIS menthod

In order to better illustrate the difference between the parameter settings recommended in the STAR-CCM+ *Instructions for User* file (referred to in the following as the 'official recommendations') and the parameter settings for Sample 3 (referred to as 'our recommendations'), Fig. 14(a) shows the nominal wake at 0.1RP behind the propeller, and Fig. 14(b) presents the effective wake calculated using the official recommendations, with our recommendations shown in Fig. 14(c). The propeller speed is 10 rps. Table 7 shows the error between the CFD results and the EFD results for the two parameter settings. The error transfer method is based on Eq. (27). The speed of the ship model is selected as the operating speed V = 1.035 m/s, n is the propeller rps at the self-propulsion point, T is the thrust at the self-propulsion point, t is the thrust reduction coefficient, K_T is the thrust coefficient, J is the propeller advance speed, Q is the propeller torque, ω represents the wake fraction, η_{Hm} is the hull efficiency, η_{0m} is the propeller efficiency, and η_D is the propulsion efficiency. It can be seen from Table 7 that most of the parameters, and especially the results for the wake fraction, have been significantly optimised, and our recommended values effectively reduce the error caused by the officially recommended values.

Thrust reduction and wake fraction are important parameters reflecting the interaction between the hull and propeller. The error in the wake fraction for the officially recommended value reaches 20%. For the type of ship considered in this study, the officially recommended inflow plane radius is too large, which leads to weakening of the influence of the hull on the propeller. Our recommended parameter settings and the official recommendations are all accurate in the prediction of thrust reduction, which also shows that BFM has a good effect in terms of predicting the effect of the propeller on the hull.

APPLICATION

In order to verify the applicability of the optimal inflow plane parameter setting determined in this study, another full-formed ship was selected for simulation of self-propulsion and comparison of the model test data. The C_b for this type of ship is 0.917, a higher value than for the ship considered in the previous sections. The hull form is wider, and the width-to-draft ratio B/d for this ship is also larger than for the original ship. The backup propeller for the laboratory (WUT-PM-001), which belongs to the MAU series, was used in this case. The basic parameters of the ship model and propeller are shown in Table 8. The Reynolds number of the full-scale ship and the ship model is converted at the operating speed (V = 0.703 m/s). The three-dimensional model of the hull and the ship model are shown in Fig. 15. Due to the high draught of the ship model, in order to ensure the safety of the model tests, we heightened the bulwark and bow of the test ship model, while the lower part of the waterline was completely consistent with the three-dimensional model. The open water curve for WUT-PM-001 is shown in Fig. 16.

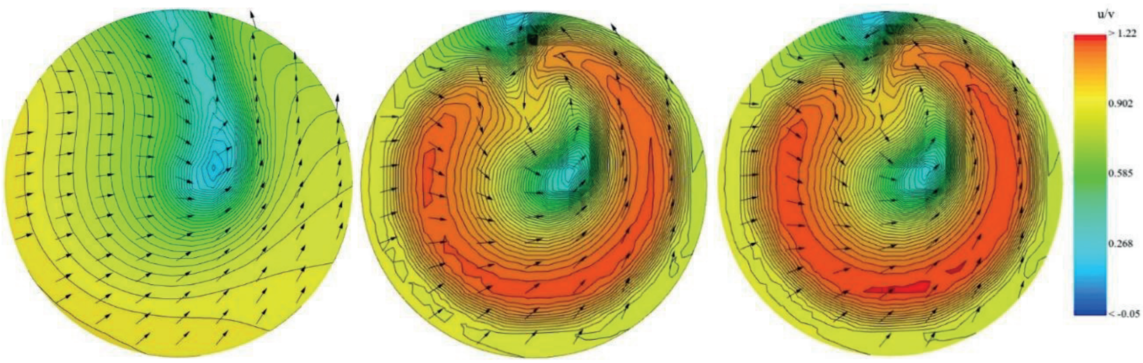

(a) *(b)* *(c)*

Fig. 14. Nominal wake and effective wake at 0.1R_p behind the propeller: (a) nominal wake; (b) effective wake obtained with official recommendations; (c) effective wake obtained with our recommendations

Tab. 7. Comparison of two sets of inflow plane parameter settings

Self-propulsion factors		n	T	t	KT	J	Q	ω	η_{0m}	η_{Hm}	η_D
Units		rps	N				$N \cdot m$				
EFD		9.48	5.95	0.21	0.10	0.55	0.12	0.20	0.66	0.99	0.65
Official recommendations	CFD	9.66	5.91	0.22	0.10	0.56	0.12	0.16	0.69	0.93	0.63
	Error (%)	2.24	0.40	8.39	3.96	2.97	10.85	20.83	4.18	7.14	3.11
Our recommendations	CFD	9.36	5.91	0.22	0.10	0.55	0.12	0.21	0.68	0.98	0.66
	Error (%)	1.30	0.67	5.20	2.14	0.51	1.32	3.30	2.97	0.58	2.52

Tab. 8. Main parameters of the ship and propeller for comparison

Parameter	Symbol	Units	Full-scale ship	Model ship
Hull				
Waterline length	L_{wl}	m	89.90	3.996
Length between Perpendiculars	L_{pp}	m	88.40	3.929
Beam	B	m	15.76	0.70
Draft	T	m	5.22	0.2320
Displacement	Δ	t	6555	0.5755
Reynolds number	Re		3.18×10^8	2.98×10^6
Block coefficient	C_b		0.917	
Scale ratio	λ		22.5	
Propeller				
Propeller type			MAU	
Propeller diameter	D	m	0.120	
Blade area ratio	A_E/A_0		0.55	
Pitch ratio	$P_{0.7}/D$		0.76	
Number of blades	Z		4	
Skew angle	θ	deg	0	
Rake angle	ε	deg	10	
Hub diameter ratio			0.18	

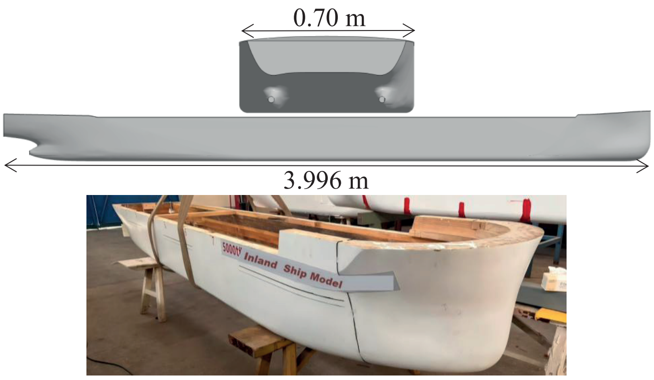

Fig. 15. Three-dimensional model of the comparison ship and the physical model

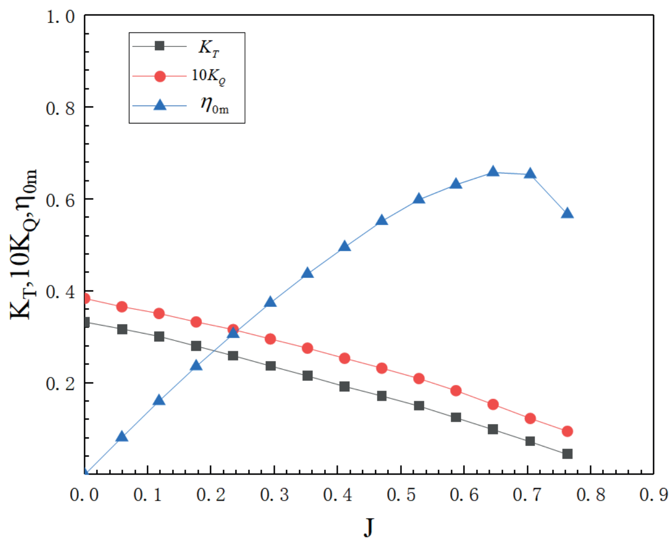

Fig. 16. Results of open water tests of the propeller for the alternative ship

Four speeds were selected for the self-propulsion simulation. The inflow plane parameters were set to our recommended values for Sample 3 ($r' = 0.8R_p$, $\Delta L = 0.2R_p$) and the officially recommended values ($r' = 1.2R_p$, $L = 0.2R_p$), and simulation calculations were performed under these two parameter settings. Figs. 17(a), (b) and (c) allow for a comparison of the simulation results and the experimental results under these two parameter settings for the thrust reduction coefficient t, the wake fraction ω and the propeller efficiency η_{0m}. The results obtained from our recommended values are represented by the red line, while those obtained with the officially recommended values are represented by the blue line. From an analysis of Fig. 17, it can be seen that the difference between the two parameter setting methods is small for the prediction of thrust reduction. Compared with the test results, the overall change trend is the same as for the test results. At the third speed point, the error for our recommended setting method is slightly higher than for the official method; however, based on the results of the four speed points, the average error in our setting method is lower than for the official method. In regard to the prediction of the wake fraction and propeller efficiency, the error obtained with our recommended method is smaller than for the official method, and the trends in the simulation results obtained according with our method with a change of speed are essentially consistent with those for the test values. When the officially recommended value is used to set the inflow plane, the trends in the simulation results for the wake fraction and thrust reduction are quite different from that of the test values.

From the comparative analysis given above, we can see that when calculating the self-propulsion of a ship with a large square coefficient using BFM, the parameter setting for the inflow plane recommended in the STAR-CCM+ *Instructions for User* file is not the most optimal. For the full-formed ship considered in this study, with $C_b \geq 0.85$, an invisible bulbous bow, a double stern, and no appendages, our recommended parameter setting is more applicable.

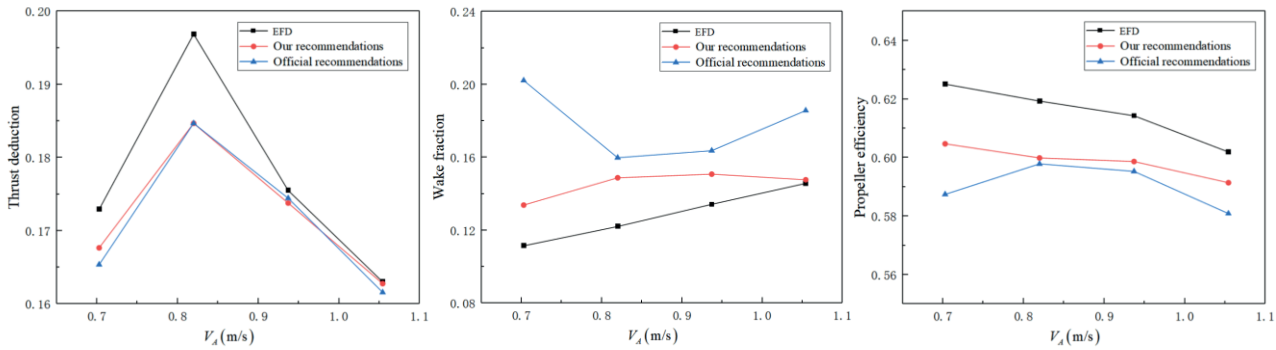

(a) (b) (c)

Fig. 17. Comparison of the optimal value of propulsion efficiency with the official reference value: (a) thrust deduction; (b) wake fraction; (c) propeller efficiency

CONCLUSION AND FUTURE WORK

In this study, we aimed to improve the accuracy of the block coefficient $C_b \geq 0.85$ for a full-formed ship in a self-propulsion simulation of body force. A full-formed ship was taken as the research object, and a self-propulsion simulation based on BFM was carried out in which we set different inflow plane parameters. The simulation results were compared with experimental results, and the influence of the inflow plane parameter setting on the self-propulsion simulation results was analysed. Finally, the TOPSIS method was used to determine the optimal parameter setting for the inflow plane suitable for the full-formed ship, in order to improve the accuracy of the simulation based on BFM. We also compared and analysed the simulation results and model test results for another full-formed ship, to verify the applicability of the inflow plane parameter setting value proposed in this study for a full-formed ship.

The main conclusions of this study are as follows:

(1) A change in the inflow plane radius and offset will affect the results of the self-propulsion simulation. The maximum error between different parameter settings can reach 36.25%. For a given inflow plane radius, when the inflow plane offset is increased, the propeller thrust, torque and hull resistance show an increasing trend.

(2) The influence of the inflow plane parameters on propeller thrust T, torque Q and hull resistance R at the same propeller speed is equivalent, and the trends in the variation of these three monitoring values are consistent.

(3) With an increase in the inflow plane offset, the peak value of the wake velocity increases.

(4) Considering the influence factors of each propulsion efficiency, when BFM is used for the simulation calculation of a full-formed ship similar to the one in this study ($C_b \geq 0.85$, with invisible bulbous bow and double stern, and no appendage), the inflow plane parameters are set as follows: inflow plane radius $r' = 0.8R_p$, offset $\Delta L = 0.2R_p$.

Our discussion of the influence of the inflow plane parameters in this study primarily involves full-formed ships. This work did not take into account the influence of multiple types of ship, and the number of samples used was small. The recommended parameter settings obtained here are mainly for full-formed ship types, where $C_b \geq 0.85$ and the ship has an invisible bulbous bow and double stern. To explore the best settings for all types of full-formed ships, a method based on mechanical learning could be used to count a large number of ship samples.

FUNDING SOURCES

This work was financially supported through "The key technology research and engineering demonstration of green and intelligent ships in the Xijiang River" (Grant GuikeAA23023013) from the Guangxi Science and Technology Major Program. It was also financially supported through the "Research and application of key technologies for green standard ship design and manufacturing" (Grant GuikeAA23062037) from the Guangxi Science and Technology Major Program.

DECLARATION OF COMPETING INTEREST

The authors declare that they have no known competing financial interests or personal relationships that could have appeared to influence the work reported in this paper.

REFERENCES

1. Guo C, Zhong X, Zhao D. Research on scale effect of resistance components for full-formed ship based on large-scale model towing test. *Journal Of Marine Science And Engineering* 2023, vol. 11, no. 7, p. 16. doi:10.3390/jmse11071300

2. Hatano S, Mori K, Hotta T. Experimental and theoretical investigation of ship boundary layer and wake. In: *Proceedings of the 12th Symposium on Naval Hydrodynamics.* Washington DC, 1978. doi:10.17226/18592

3. Peng H, Ni S, Qiu W. Wave pattern and resistance prediction for ships of full form. *Ocean Engineering* 2024, vol. 87, pp. 162-173. doi:10.1016/j.oceaneng.2014.06.004

4. Gong J, Li Y. The prediction of hull gesture and flow around ship based on Taylor expansion boundary element method. *Polish Maritime Research* 2019, vol. 26, no. 2, pp. 198-211. doi:10.2478/pomr-2019-0039

5. Tu TN, Luu DD, Nguyen THH, Nguyen TTQ, Nguyen MV. Numerical prediction of propeller-hull interaction characteristics using RANS Method. *Polish Maritime Research* 2019, vol. 26, no. 2, pp. 198-211. doi:10.2478/pomr-2019-0036

6. Acanfora M, Altosole M, Pennino S. A numerical model of ship manoeuvring for the KVLCC2 hull, in regular and long-crested irregular waves. *Ocean Engineering* 2025, vol. 333, p. 121579. doi:10.1016/j.oceaneng.2025.121579

7. Degiuli N, Marti I, Bua MP, Grlj CG. Benchmark study on resistance and propulsion characteristics of a 6750-TEU container ship. *Ocean Engineering* 2025, vol. 319, p. 120300. doi:10.1016/j.oceaneng.2025.120300

8. Themelis N, Nikolaidis G, Zagkas V. Assessment of hull and propeller degradation due to biofouling using tree-based models. *Applied Sciences* 2024, vol. 14, no. 20, p. 9363. doi:10.3390/app14209363

9. Tang SX, Duan WY, Chen JK. Self-propulsion performance prediction in calm water based on RANS/TEBEM coupling method. *Engineering Analysis with Boundary Elements* 2024, 169, Part A. doi:10.1016/j.enganabound.2024.105979

10. Jin Y, Duffy J, Cai SH, Magee AR. DTMB 5415M dynamic manoeuvres with URANS computation using body-force and discretised propeller models. *Ocean Engineering* 2019, vol. 182, pp. 305-317. doi:10.1016/j.oceaneng.2019.04.036

11. Li S, Liu C, Chu X, Zheng M, Wang Z, Kan J. Ship maneuverability modeling and numerical prediction using CFD with body force propeller. *Ocean Engineering* 2022, vol. 182, no. 264, p. 112454. doi:10.1016/j.oceaneng.2022.112454

12. Liu Z. Analysis of the accuracy of a body-force propeller model and a discretized propeller model in RANS simulations of the flow around a maneuvering ship. *Journal of Marine Science and Engineering* 2025, 13. doi: 10.3390/jmse13040788

13. Knight BG, Maki KJ. A semi-empirical multi-degree of freedom body force propeller model. *Ocean Engineering* 2019, vol. 178, pp. 270-282. doi:10.1016/j.oceaneng.2019.02.056

14. Chuan TQ, Phuong NK, Tu TN, Quan MV, Anh ND, Le TH. Numerical study of effect of trim on performance of 12500DWT cargo ship using Ranse method. *Polish Maritime Research* 2022, vol. 29, pp. 3-12. doi:10.2478/pomr-2022-0001

15. Zhang Y, Windén B, Ojeda HRD, Hudson D, Turnock S. Influence of drift angle on the propulsive efficiency of a fully appended container ship (KCS) using computational fluid dynamics. *Ocean Engineering* 2024, vol. 292, p. 116537. doi:10.1016/j.oceaneng.2023.116537

16. Islam H, Soares CG. Estimation of hydrodynamic derivatives of an appended KCS model in open and restricted waters. *Ocean Engineering* 2022, vol. 266, p. 112947. doi:10.1016/j.oceaneng.2022.112947

17. Song S, Kim D, Dai S. CFD investigation into the effect of GM variations on ship manoeuvring characteristics. *Ocean Engineering* 2024, vol. 291, p. 116472. doi:10.1016/j.oceaneng.2023.116472

18. Guo C, Wang X, Wang C, Zhao Q, Zhang HP. Research on calculation methods of ship model self-propulsion prediction. *Ocean Engineering* 2020, vol. 203, p. 107232. doi:10.1016/j.oceaneng.2020.107232

19. Feng D, Yu J, He R, Zhang Z, Wang X. Improved body force propulsion model for ship propeller simulation. *Applied Ocean Research* 2020, vol. 104, p. 102328. doi:10.1016/j.apor.2020.102328

20. Cai B, Mao X, Xu Q, Cai W, Tian B, Qiu L. Simulation of the interaction between ship and ducted propeller with a modified body force method. *Ocean Engineering* 2022, vol. 249, p. 110950. doi:10.1016/j.oceaneng.2022.110950

21. Yu J, Yao C, Liu L, Zhang Z, Feng D. Assessment of full formed KCS free running simulation with body-force models. *Ocean Engineering* 2021, vol. 237, p. 109570. doi:10.1016/j.oceaneng.2021.109570

22. Aram S, Mucha P. CFD validation and analysis of turning maneuvers of a surface combatant in regular waves. *Ocean Engineering* 2024, vol. 293, p. 116653. doi:10.1016/j.oceaneng.2023.116653

23. Xie C, Zhou L, Ding S, Lu M, Zhou X. Research on self-propulsion simulation of a polar ship in a brash ice channel based on body force model. *International Journal of Naval Architecture and Ocean Engineering* 2023, vol. 15, p. 100557. doi:10.1016/j.ijnaoe.2023.100557

24. Cai B, Qiu L, Tian B, Xu Q, Mao X, Chai W, Zhan X. Research on predicting methods of propeller-hull interactions in head waves. *Ocean Engineering* 2023, vol. 269, p.113493. doi:10.1016/j.oceaneng.2022.113493

25. STAR-CCM+ Theory Guide. CD ADAPCO, 2021. Retrieved from: https://www.sw.siemens.com/

26. Reissner H. On the vortex theory of the screw propeller. *Journal Of the Aeronaut Sciences* 1937, vol. 5, no. 1, pp. 1-7. doi:10.1098/rspa.1929.0078

27. Hough GR, Ordway D. The generalized actuator disk. Therm. Advanced Research Inc., Ithaca, NY; 1964. doi: 10.21236/ad0433976

28. Stern F, Wilson R, Shao J. Quantitative V&V of CFD simulations and certification of CFD codes. *International Journal for Numerical Methods in Fluids* 2006, vol. 50, no. 11, p. 1335e1355. doi:10.1002/fld.1090